Inquiro, the UAB undergraduate science research journal

Volume 2014 | Number 8 Article 21

2014

Characterization and Development of BaZrO3/NiO Composites for Use as Anodes in Proton Conducting SOFCs

Islam Khan

Kelly Dillon

Amber Genau

Renato Camata

Characterization and Development of $BaZrO_3$/NiO Composites for Use as Anodes in Proton Conducting SOFCs

Islam Khan[1], Kelly Dillon[2], Amber Genau[2], and Renato Camata[1]

[1]Department of Physics, University of Alabama at Birmingham, Birmingham, AL, USA
[2]Department of Materials Science and Engineering, University of Alabama at Birmingham, Birmingham, AL, USA

Abstract

Solid oxide fuel cells (SOFCs) are devices that directly convert chemical into electrical energy through oxidation of a fuel. Currently, there is intense interest in developing new kinds of SOFCs that can reduce the typical 800 °C to 1000 °C operating temperature of existing cells to the more manageable 400 °C to 600 °C range, which can be achieved by using doped perovskite-type $BaZrO_3$ protonic conductors as the electrolyte. However, no effective anode materials that are compatible with $BaZrO_3$ have yet been demonstrated. The focus of this work is on developing and characterizing anode materials suitable for integration with $BaZrO_3$-based electrolytes, to enable the next generation of SOFCs. The anode material selected for study was $BaZrO_3$-Ni cermet (ceramic and metal). Samples were created by mechanically mixing $BaZrO_3$ and NiO powders, followed by pressing into cylindrical pellets (0.5 inch in diameter), and sintering at various temperatures. Hypothesizing that the properties of the initial composite $BaZrO_3$-NiO have a strong influence on the properties of the $BaZrO_3$-Ni obtained after reduction in hydrogen, we studied NiO and $BaZrO_3$-NiO composites as a first step to characterizing these complex materials. Grain growth and porosity were observed in BaZrO3-NiO using optical microscopy image analysis, and results showed that 1400 °C to 1600 °C is a suitable sintering temperature range for these composites, with the porosity in their microstructures remaining relatively constant beyond 1500 °C. Electrochemical impedance spectroscopy (EIS) that was carried out on NiO as a reference indicated that there are multiple factors that contribute to the impedance in its structure, and possible sources for each factor are discussed.

Keywords: Solid oxide fuel cells (SOFCs), Anode, Barium zirconate ($BaZrO_3$), Nickel oxide (NiO), Electrochemical impedance spectroscopy (EIS)

Introduction

Today, most of the world's energy is obtained from fossil fuels. However, fossil fuels are slowly being depleted. As the world ages and the population grows, the balance between supply and demand of energy shifts. The modernization and industrialization of previously underdeveloped countries increases further the demands for energy currently obtained from fossil fuels by the method of combustion, creating more air pollution. The rate of growth of world demand for energy is much faster than the rate of replenishment of traditional energy sources. The urgency to fulfill the demand for energy and the increased awareness of global warming has prompted research seeking alternative energy sources that are affordable, reusable, and less harmful to the environment.

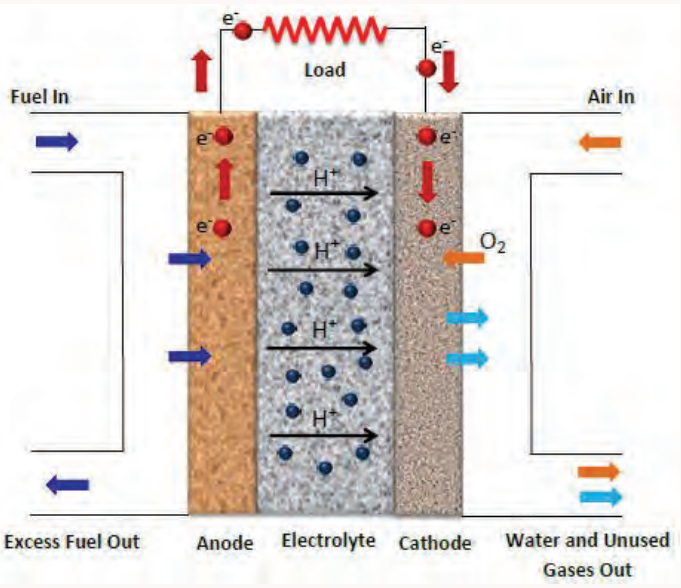

Figure 1. Schematic diagram of a protonic solid oxide fuel cell (SOFC).

One alternative is the use of fuel cells, which are devices that convert chemical energy into electrical energy directly through various mechanisms. One type of fuel cell is the solid oxide fuel cell (SOFC) which uses an oxide material as the electrolyte and oxidation of the fuel to convert energy from chemical to electrical form.[1] Hydrogen fuel and oxygen are used in SOFCs to generate electric current with water as a byproduct (Figure 1). As H_2 molecules in the gas phase enter the anode and pass through porous networks, a chemical reaction takes place at the triple phase (anode, electrolyte, and H_2) boundary regions. Due to high temperature, H_2 molecules are split into H^+ ions (protons) and electrons. The O_2 molecules from air entering through the cathode on the opposite side of the fuel cell combine with these electrons

and the protons that have diffused through the electrolyte to form water as the end product. A continuous conversion to electrical energy can be obtained through a constant flow of electrons, provided that a continuous source of H_2 and air is fed to the fuel cell.

Solid oxide fuel cells have a number of advantages over fossil fuels. They are highly efficient, sustainable, and produce lesser quantities of greenhouse gases.[2] Compared to the efficiency of gasoline internal combustion in a car engine, which is about 20 – 25 %, fuel cells used in a vehicle can have an energy conversion efficiency of about 64 %, which is significantly higher. The most established SOFC technology is based on a yttria-stabilized zirconia (YSZ) electrolyte, which requires the cell to operate at high temperatures (800 °C to 1000 °C).[3,4] These high operating temperatures demand expensive materials for the fuel cell interconnectors, cause thermal stress, require long start-up times, and require substantial energy inputs to heat the cell up to the operating temperature.[5] Consequently, there is a need to reduce the operating temperature to support the use of SOFCs for widespread applications. There is an intense interest in developing new kinds of SOFCs that can reduce the typical 800 °C to 1000 °C operating temperature of existing cells to the more manageable 400 °C to 600 °C temperature range. This can be achieved by creating better electrolytes or better electrodes within the SOFCs that can operate at a lower temperature.[1]

Materials science research has been mainly focused on oxygen-ion conductor electrolyte alternatives to YSZ for many years. However, in recent years, interest has been driven toward proton-conducting ceramics, in particular oxides with perovskite-type structure ABO_3 in which the A site contains alkaline earth elements and the B site contains tetravalent elements.[5] It has been reported that proton-conducting oxides perform well in intermediate temperatures (400 °C to 700 °C) and display higher conductivity measurements along with a lower activation energy compared to the standard oxygen-ion conducting electrolytes.[6]

The main focus of this research is to investigate possible anode materials for proton-conducting SOFCs. An ideal anode for SOFCs is a good electrical conductor for the transfer of electrons, has a porous structure that allows the H_2 to pass through the anode structure and react at the anode's interface with the electrolyte, and has a similar coefficient of thermal expansion (CTE) to that of the electrolyte in order to have lattice compatibility. The most common anodes in the SOFC community are made of an electrolyte-NiO composite material.[7] The electrolyte-NiO composites are reduced in H_2 to remove the oxygen atoms in the NiO to form an electrolyte-Ni composite material which is composed of a ceramic and a metal, commonly known as cermet. The reason electrolyte-Ni cermet is used as an anode is because Ni has a high CTE compared to that of most electrolytes being used in fuel cells and this would result in uneven thermal expansion and contraction at the anode/electrolyte interface. This electrolyte-Ni combination of $BaZrO_3$-Ni greatly lowers the CTE of the anode which shows compatibility with the electrolyte, thus enabling anode-supported SOFCs to be made.

Doped barium cerate ($BaCeO_3$) and doped $BaZrO_3$ are the two most investigated proton-conducting materials. Unlike doped $BaCeO_3$, $BaZrO_3$ has shown high chemical stability against H_2O and CO_2 and high proton conductivity.[6] Thus, the usage of $BaZrO_3$ as a high temperature proton conductor is common among researchers. We hypothesize that the properties of the intermediate composite materials $BaZrO_3$-NiO have a strong influence on the final properties of the $BaZrO_3$-Ni cermet anode. Our goal is to study these composite materials and develop a good anode material with good electronconductivity, controlled porosity in the microstructure, and CTE compatibility with the electrolyte in SOFCs.

Materials and Methods

$BaZrO_3$ and NiO (BZ/NiO) composite pellet samples were made using a mechanical mixing method. The BZ powders used had a density of 5.52 g mL^{-1} at 25 °C and had a particle size of less than 10 µm. The NiO powders used had particle sizes of 12 µm to 22 µm. A mortar and pestle was used to thoroughly mix the two powders, then the mixture was pressed using a 12.7 mm I.D. pressing die set and hydraulic press. The pressure applied on the powder mixtures was 12000 psi (82.737 MPa). The samples were then placed in a furnace and sintered in air at 1500 °C for 5 h. Each side of the pellet samples was polished using a metallographic polishing machine: silicon carbide sandpaper with grit size 800 was used, followed by sandpaper with grit size 1200, and finally a polishing cloth with 1 µm diamond paste. Multiple pellet samples with different ratios by weight were made using this procedure. Optical microscopy was used to take images of the surfaces of the composite sample. Images with magnifications of 200x and 500x were obtained. With the intention to look closer at the microstructure of the composite sample, scanning electron microscopy (SEM) was used to carry out back-scattered electron (BSE) imaging as well as secondary electron (SE) imaging on the sample. Energy-dispersive x-ray (EDX) spectroscopy was used to carry out an elemental analysis on the different phases that appeared on the surfaces of the samples.

Furthermore, five BZ/NiO pellet samples with 40/60 ratio by weight were made using the same procedure except that the sintering temperature was varied from 1300 °C to 1700 °C in 100 °C increments while keeping all other parameters constant. The samples were polished using the same procedure as before, and images of both sides of each sample were obtained using optical microscopy. Twenty

images, ten from each side, of each of the samples were used for the purpose of measuring the porosity as a function of temperature. Using image analysis software Image-Pro Plus, a color threshold was applied on the images to visually highlight the dark regions on the images that represented the pores. This highlighted area was used to measure the percentage of porosity per unit area for each of the selected areas of the sample. The porosity percentage of each of the five samples was estimated by calculating an average of the porosity percentages of all twenty images per sample and the results were compared and analyzed. A pure BZ pellet sample and a pure NiO pellet sample were also made using the same procedure. The sintering temperature used for both pellet samples was 1500 °C, and the sintering time was 5 h. X-ray diffraction (XRD) analysis was carried out on the pure BZ, the NiO, and 40/60 BZ/NiO pellet samples sintered at 1300 °C and 1500 °C. This analysis was carried out in order to test the purity of the sintered composite pellets by comparing the diffraction patterns of BZ and NiO reference data obtained from the American Mineralogist Crystal Structure Database (AMCSD) with that of the BZ, NiO and the two 40/60 BZ/NiO pellet samples that were obtained by taking XRD measurements.

A pure NiO pellet sample with particle size 0.5 µm to 1.5 µm was made as a reference by using hot press (350 °C for 2 h) followed by sintering at 1500 °C for 5 h. In order to create contacts on the composite sample as well as the pure NiO sample, Ni was deposited on both sides of each sample using pulsed laser deposition (PLD). The pellets were then placed between two electrodes, and a staircase potentio electrochemical impedance spectroscopy (SPEIS) sweep was carried out on each of them to measure their electrical properties. The frequency was varied in the range 1 Hz to 7 MHz, and the voltage was varied in the range 0 V to 10 V in 0.5 V increments.

The complex plane of Nyquist plots (Re(Z) vs –Im(Z)) obtained from the Electrochemical Impedance Spectroscopy (EIS) was thoroughly analyzed. A mathematically equivalent circuit model was used to fit the model data on the measured data and values of resistances were obtained. A bode plot (|Z| vs frequency) was also obtained and the capacitance for each voltage was obtained using the equivalent circuit model. A capacitance versus voltage graph (C vs. V) was obtained followed by the reciprocal of capacitance square versus voltage graph ($1/C^2$ vs. V). The slope of this graph was used to calculate the charge carrier concentration in the NiO using the following equation:

$$n = \frac{2}{q\varepsilon A^2 \frac{1}{\frac{d}{dV}\left(\frac{1}{C^2}\right)}} \qquad (1)$$

Results and Discussion

The images of the 60/40 BZ/NiO sample obtained using optical microscopy showed the presence of three different phases of materials along with pores in their microstructures. The porosity in the microstructure was a defect that resulted from the incomplete densification of the powder particles during sintering. Figure 2a shows one of these images in which the brighter regions were in the NiO phase, and the grey regions were in the BZ phase. There were also dark grey regions whose phase was unknown at first. EDX spectroscopy analysis on those regions gave the same elemental composition as the grey regions that were in the BZ phase. The SE detector was divided into quadrants, and subtraction of two opposite quadrants was used to obtain topographical images that show the surface of the composite pellet to be fairly smooth except at the dark grey regions where shallow holes occurred. It was hypothesized that the depth of these holes resulted in those regions appearing darker in both the optical microscope and SEM images.

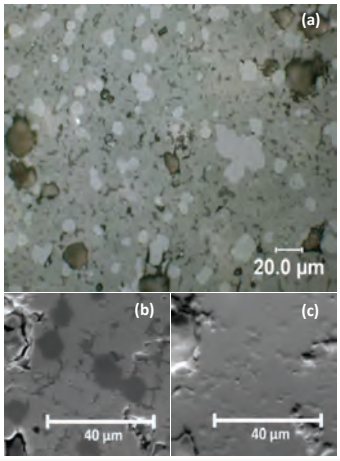

Figure 2. (a) Optical microscopy image of 60/40 BZ/NiO sintered at 1500 °C for 5 h showing the different phases. (b) Scanning electron microscopy (SEM) image in secondary electron mode. (c) Topographical image obtained using back-scattered electron mode in SEM.

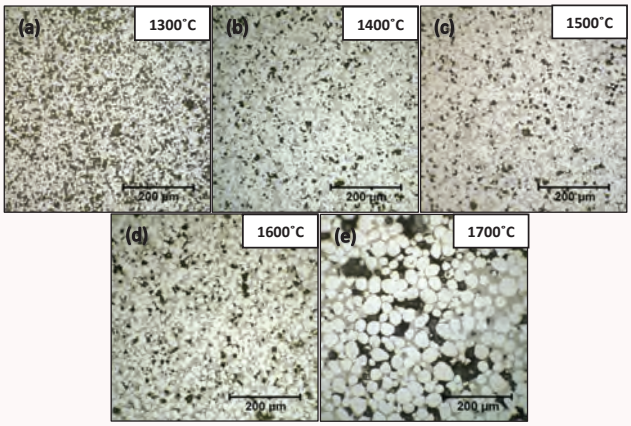

Figure 3. Optical microscopy images of 40/60 BZ/NiO sintered for 5 h at (a) 1300 °C (b) 1400 °C (c) 1500 °C (d) 1600 °C and (e) 1700 °C.

As seen in Figure 3, optical microscopy analysis of the five 40/60 BZ/NiO samples that had been sintered at different temperatures showed that the samples sintered at higher temperatures had a larger grain growth as well as less porosity per unit area compared to the samples that had been prepared at lower temperatures. It was noted that even though the same procedure was used to polish both the samples, the sample sintered at a higher temperature appeared shinier on the surface, possibly due to the reduction in porosity. The larger grain growth and higher densification at the higher temperature were expected since there was more thermal energy available for atomic diffusion to take place in the microstructure. The sample sintered at 1700 °C showed evidence of non-uniformity in porosity in the microstructure of the composite. The BZ phase was observed to be more concentrated at certain areas, leaving large pores behind. Figure 3 shows images of the five samples obtained using optical microscopy at a magnification of 200x.

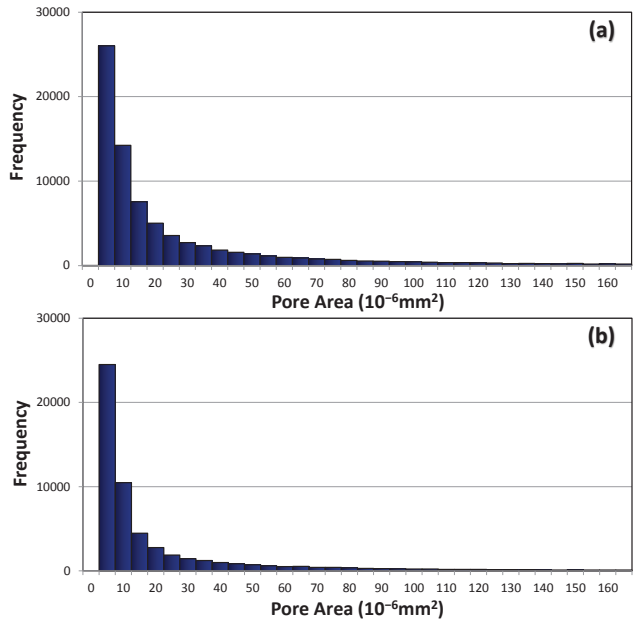

Figure 4. Pore area distribution of 40/60 BZ/NiO samples sintered at (a) 1300 °C and (b) 1500 °C.

The porosity of each side of the 40/60 BZ-NiO samples was measured using image analysis. The samples sintered at 1300 °C, 1400 °C, 1500 °C, 1600 °C, and 1700 °C showed an average porosity of 28.3 % ± 2.4 %, 10.2 % ± 1.4 %, 16.9 % ± 2.3 %, 17.0 % ± 1.0 %, and 16.8 % ± 3.7 %, respectively. These results show that the porosity appears to be highly uniform across each of the samples sintered at lower temperatures. Figure 4 displays the pore size distribution for the two samples that were sintered at 1300 °C and 1500 °C. About 94 % of the pores were 1.65 × 10^{-4} mm^2 or smaller for the sample sintered at 1300 °C, and 96 % of the pores were 1.65 × 10^{-4} mm^2 or smaller for the sample sintered at 1500 °C. The porosity in the composites has been summarized in a histogram in Figure 5. The histogram shows that the porosity decreases with the increase in temperature, but beyond 1500 °C the porosity percentage remains relatively constant with the increase in temperature. The high standard deviation in the porosity percentage measurements for the sample sintered at 1700 °C also indicates the non-uniformity of pores in the composite microstructure.

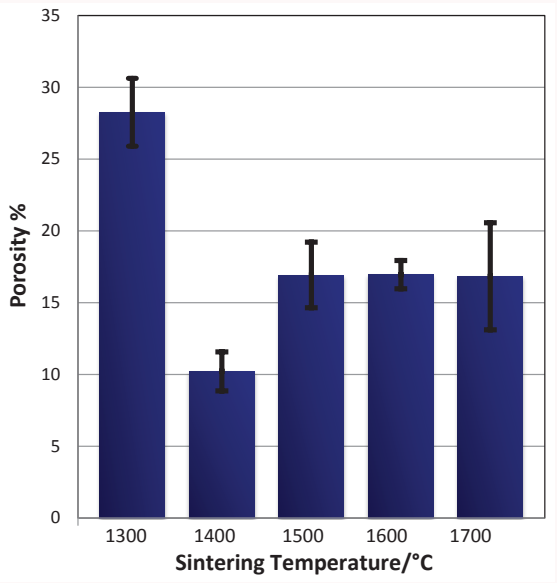

Figure 5. Histogram showing porosity percentage of 40/60 BZ/NiO as a function of sintering temperature. The error bars represent standard deviation.

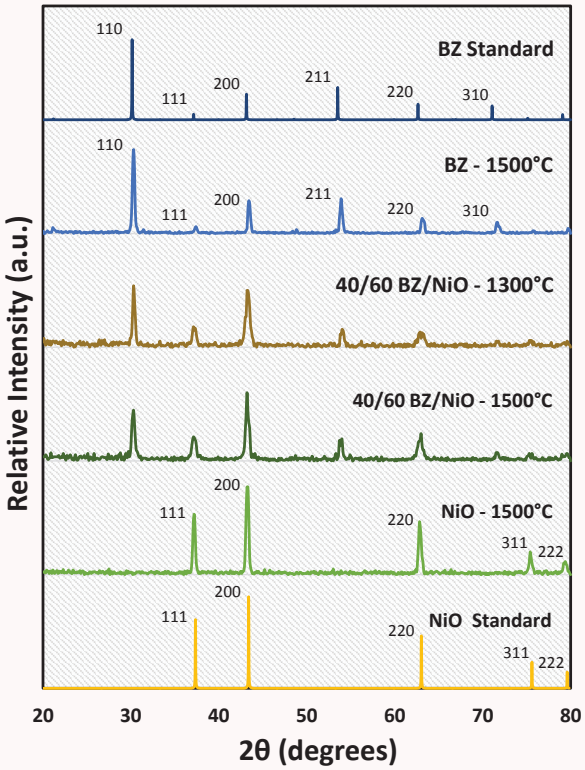

Figure 6. XRD patterns of BZ, NiO and 40/60 BZ/NiO composites sintered at different temperatures with reference data obtained from AMCSD.

The XRD patterns of the four pellet samples along with the reference XRD patterns of BZ and NiO obtained from the AMCSD are shown in Figure 6. Results show that the BZ and NiO pellet samples prepared by firing at 1500 °C for 5 h had the same phases as in the reference XRD patterns, indicating that there were no changes in phase during the sintering process. The XRD patterns of the two 40/60 BZ/NiO composite pellet samples fired at 1300 °C and 1500 °C cannot be differentiated. In both cases, the peaks appear only at those values of 2θ at which the peaks appear for the BZ and NiO pellet samples. This indicates that the two phases in the composite, BZ and NiO, retained their phases after they had been sintered, which also indicates that there are no reactions taking place between the two phases in the composite or between the composites and the air present in the furnace during the sintering process.

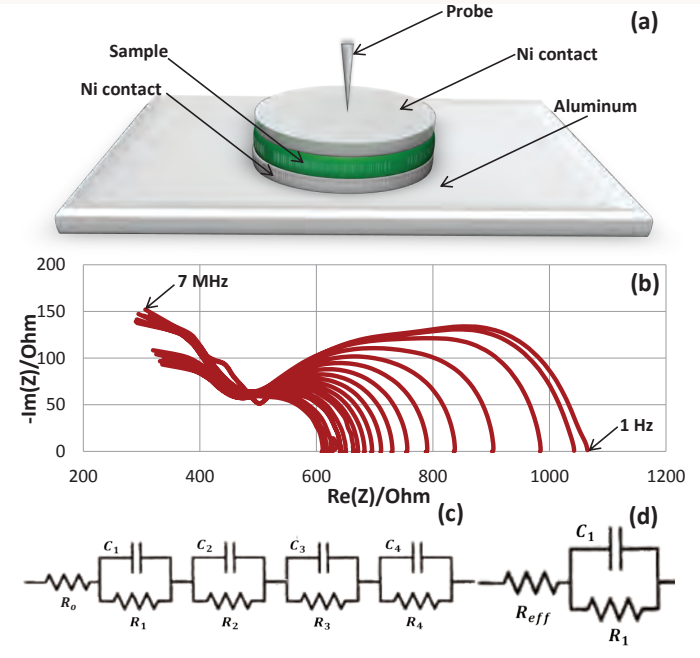

Figure 7. (a) Graphic showing the system used for taking impedance measurements. (b) Complex-impedance plane plot for the NiO. (c) Equivalent circuit model used to measure resistance and capacitance. (d) Simplified equivalent circuit model assuming the polarization is due to the electrode/NiO interface.

The electrical properties of a material are commonly studied by measuring the magnitude of opposition to electric current through it. NiO is known as a p-type semiconductor with a wide band gap that conducts a negligible amount of current at room temperature.[9,10] However, an alternating current (AC) can be conducted through a dielectric (insulating material) by the polarization mechanism. Like resistance is the opposition to direct current (DC), impedance is the opposition to AC that provides valuable information regarding the electrical properties of a dielectric material. Figure 7a shows a schematic of the system that was used to take impedance measurements on the samples. In EIS, an electrical stimulus (known voltage or current) over a range of frequencies is applied and the response of the system is observed. Different polarization mechanisms in a system are only activated at certain frequencies. The complex-impedance plane/Nyquist plot for the pure NiO sample pellet with Ni contacts on both sides was obtained (Figure 7b). In a typical Nyquist plot, each polarization in the system corresponding to different dielectric mechanisms gives rise to a semicircle with a single time constant. Impedance measurements on BZ/NiO composites proved to be too difficult to comprehend since there are two phases of materials in the structure. Therefore, the system was simplified by taking impedance measurements on pure NiO samples that only contained one phase. The complex-plane plot of NiO is complicated compared to typical plots which have clearly defined semicircles. Looking at the results, four overlapping indistinct semicircles can be observed with some difficulty. Mathematically equivalent circuit models can be designed to give similar plots as a real system that produces semicircles in a Nyquist plot. Figure 7c shows the equivalent circuit model that was used to fit the curve on the measured data.

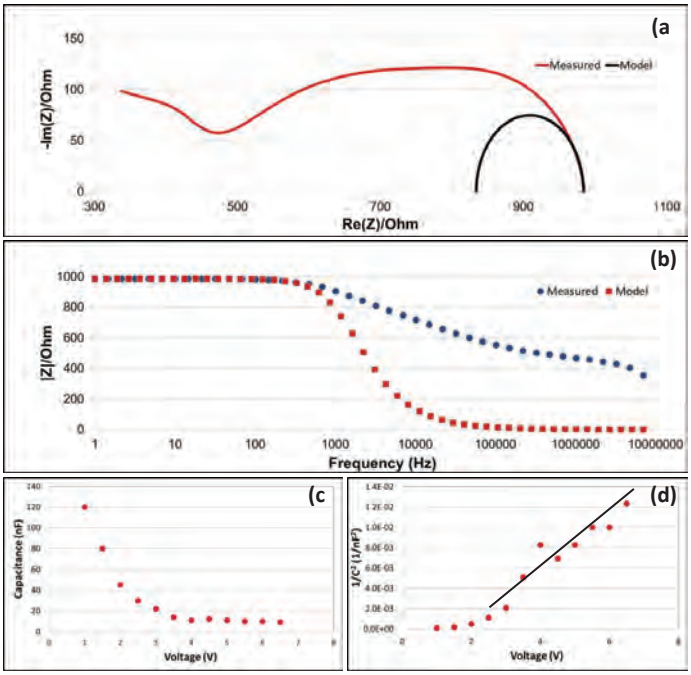

Figure 8. (a) Electrical circuit model used to fit complex plane plot on measured data to obtain resistance. (b) Model used on bode plot to measure capacitance. (c) Graph showing capacitance vs voltage. (d) Graph showing $1/C^2$ vs voltage graph the slope of which can be used to measure charge carrier concentration.

It is known that the polarization that takes place at a metal-semiconductor interface is activated at a lower frequency range. Possible sources for the other impedance can be attributed to bulk conductivity resistance and grain boundary contributions. The semicircle at the lowest frequency

also intercepts the x-axis in the Nyquist plot at 90°. Given the complexity of the Nyquist plot of NiO, an attempt for simplification was made by only taking into consideration the semicircle at the lowest frequency, which is assumed to be the polarization taking place at the Ni-NiO interface. When a metal makes a contact with a semiconductor, a barrier is formed at the metal-semiconductor interface and it is known as a Schottky barrier. Figure 9a displays the assumed band diagram of p-type semiconductor NiO indicating the vacuum energy E_{Vac}, conduction energy E_C, Fermi energy E_F, valence band E_V, electron affinity χ, work function φ, and band gap E_g in which the acceptor impurities in NiO contribute hole levels in the semiconductor band gap which shifts the Fermi level downwards at a point about halfway between the acceptor levels and the valence band. The Ni is assumed to have a higher work function, which is the energy difference between the vacuum level and the Fermi level, compared to the NiO. When they are brought into contact, their Fermi levels would align as a brief transient current flow would take place from the Ni to NiO assuming the Ni has a higher work function. The electrons that flow from the Ni to NiO get bounded to fixed positions in the NiO. This can also be seen as the NiO having an excess of positive holes and, upon contact with Ni, the holes "flow" from the NiO to the Ni, leaving negative charges behind. This flow of charges creates a depletion layer, and the accumulation of positive charges in Ni and of negative charges in NiO, both at the boundary, creates a capacitor. Figure 9b shows band diagrams of the Ni and NiO after they have been brought into contact and a Schottky barrier is created.

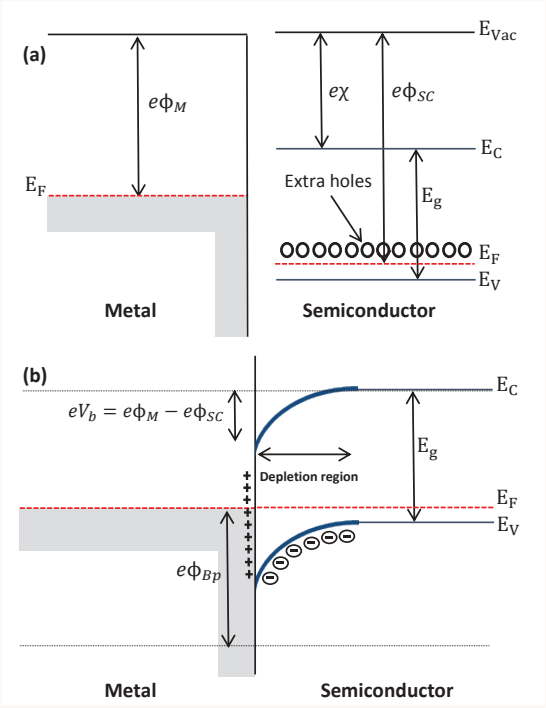

Figure 9. (a) Ni and NiO band diagrams before contact. (b) Schottky barrier after Ni and NiO are brought into contact.

The capacitor created at the Ni-NiO interface has an electric field pointing from the positive to negative charges. In the parallel plate capacitor, the capacitance resists any change in voltage and remains constant; however, the capacitance at the metal-semiconductor junction does not remain constant since the width of the depletion layer varies with the applied voltage. The increase in reverse bias adds more electrons on the NiO side of the barrier which raises its Fermi level. This increase in voltage increases the width of the depletion region. This width of the depletion region is also the separation distance between the two average planes of charges. Capacitance is inversely proportional to the distance between the planes of charges, and therefore the capacitance of the Ni-NiO Schottky barrier should decrease with the increase in voltage.

Using the simplified equivalent circuit model and method of fitting curve, the resistance for each forward bias voltage was measured and it was noted that the resistance decreased with the increase in voltage. These resistance values were used to fit the curve on the bode plot and the capacitance for each forward bias voltage was also measured. A capacitance against voltage graph was plotted and the results show that the capacitance due to the Ni-NiO interface decreases with the increase in voltage (Figure 9c), an outcome which agreed with the predictions. This shows that the assumed band diagram of the Schottky barrier is possibly correct. Furthermore, a $1/C^2$ against voltage was plotted and using the slope of this curve and Eq. 1, the charge carrier concentration in NiO was found to be 2.94×10^{10} cm^{-3} at room temperature. This is a reasonable value of charge carrier concentration for a typical semiconductor.

Conclusions

The goal of this research was to study the factors contributing to the properties of anode materials and develop a better anode for use in SOFCs. In order to reach this goal, the microstructure and electrical properties of potential materials for use in SOFCs, in particular SOFCs with solid ceramic $BaZrO_3$ electrolytes, were studied. An electrolyte-Ni cermet is generally used for anode materials because it shows good electrical conduction, catalytic activity, and CTE compatibility. $BaZrO_3$/NiO composite materials are commonly prepared by a mechanical mixing method followed by sintering at high temperatures and reducing the NiO to Ni to produce the $BaZrO_3$/Ni cermet. The microstructure and electrical properties of the $BaZrO_3$/NiO composite material plays a crucial role in the properties of the cermet and hence its function as an anode in the SOFCs. A BZ/NiO composite with 60/40 weight ratio was prepared by mechanically mixing the powders and sintering at 1500 °C for 5 h. Optical microscopy image analysis and SEM imaging showed that there are two phases (BZ and NiO) in the microstructure with the presence of porosity, which is a defect that is beneficial for use in anodes in fuel cell applications. Porosity percentage

as well as pore size distribution of five 40/60 BZ/NiO pellet samples that were sintered at different temperatures were analyzed and compared. Results show that the porosity in the samples that were sintered at lower temperatures appeared to be highly uniform but at high temperatures there is non-uniformity in the porosity in the microstructure. Uniformity in porosity is important for fuel cell applications since the fuel in gas phase needs to pass through the anode uniformly across the anode for good performance. The sample sintered at 1300 °C showed high porosity percentage which would affect the conductivity of the composite. Therefore, 1400 °C to 1600 °C is a suitable sintering temperature range for preparation of these composite materials. XRD patterns of the samples were compared with reference XRD patterns of BZ and NiO obtained from the AMCSD, and results showed that the two phases do not undergo any phase change during the sintering process and that no reaction of the two BZ/NiO composite phases takes place with each other or with air when they are being sintered. Impedance measurements on the BZ/NiO proved to be too complex to comprehend due to the presence of two phases in its structure, and therefore impedance analysis was carried out on NiO with Ni contacts on both sides that showed there are four or more sources of impedance in the system. Possible sources of impedances in the system are bulk conductivity resistance, grain boundary contributions, and Ni-NiO interface resistance. Using SPEIS, the polarization at the Ni-NiO junction was investigated and results showed that the charge carrier concentration in the NiO in the sample is about 2.94×10^{10} cm^{-3} at room temperature. The semicircles that are attributed to the Ni-NiO interface can now be subtracted from the data and the other sources of impedance investigated. Using a similar method as used for the Ni-NiO interface polarization, the values of resistance and capacitance of the other impedance contributors can be measured. A basic understanding of the BZ/NiO composites has been achieved by this research project and the next stage is to reduce this composite to BZ/Ni cermet in H_2 and study its properties. This reduction process would increase the porosity in the microstructure as oxygen atoms would be taken away from it. The porosity percentage measured in the BZ/NiO composite should be proportional to the porosity of the cermet after reduction, but the new material produced would have an electrical conductor Ni in it and would therefore have very different electrical properties compared to those of the composite. Studying the properties of the cermet would be the next step in order to develop good anode materials.

Acknowledgements

Support for this project was provided by the UAB College of Arts and Sciences Interdisciplinary Innovation Team Award entitled, "A New Interdisciplinary Research Thrust in Ceramic Materials for Clean Energy Applications with Broad Student Participation." The authors would like to thank Zack Lindsey, Eric Remington, Alex Skinner, William Warriner, and Elis Rivera for their technical assistance and support with experiments.

References

1. Fabbri, E., Bi, L., Pergolesi, D., & Traversa, E. Towards the next generation of solid oxide fuel cells operating below 600 °C with chemically stable proton-conducting electrolytes. *Advanced Materials*. 24, 195-208 (2012).
2. Traversa, E., & Boudghene Stambouli, A. Solid oxide fuel cells (SOFCs): A review of an environmentally clean and efficient source of energy. *Renew. Sustain. Energy Rev*. 6, 433-455 (2002).
3. Singhal, S. C. Advances in solid oxide fuel cell technology. *Solid State Ionics*. 135, 305-313 (2000).
4. Steele, B., & Heinzel, A. Materials for fuel-cell technologies. *Nature*. 414, 345-352 (2001).
5. Fabbri, E., Pergolesi, D., & Traversa, E. Materials challenges toward proton-conducting oxide fuel cells: A critical review. *Chem. Soc. Rev*. 39, 4355-4369 (2010).
6. Bi, L., Fabbri, E., Sun, Z., & Traversa, E. Sinteractive anodic powders improve densification and electrochemical properties of BaZr0.8Y0.2O3-o electrolyte films for anode-supported solid oxide fuel cells. *Energy and Environmental Science*. 4, 1352-1357 (2011).
7. Bi, L., Fabbri, E., Sun, Z., & Traversa, E. BaZr(0.8)Y(0.2)O(3-delta)-NiO Composite anodic powders for proton-conducting SOFCs prepared by a combustion method. *Journal of the Electrochemical Society*. 158, B797-B803 (2011).
8. Morin, F. J. Electrical properties of NiO. *Phys. Rev*. 93, 1199-1204 (1954).
9. Hufner, S., Steiner, P., Sander, I., Reinert, F., & Schmitt, H. The optical gap of NiO. Z. *Phys. B - Condensed Matter*. 86, 207-215 (1992).